V European Conference on Computational Fluid Dynamics
ECCOMAS CFD 2010
J. C. F. Pereira and A. Sequeira (Eds)
Lisbon, Portugal,14-17 June 2010

THE INFLUENCE OF THE STRUCTURAL MODEL ON THE STABILITY OF COUPLING ITERATIONS IN PARTITIONED FLUID-STRUCTURE INTERACTION SIMULATIONS

Joris Degroote*, Sebastiaan Annerel* and Jan Vierendeels*

*Ghent University, Department of Flow, Heat and Combustion Mechanics,
Sint-Pietersnieuwstraat 41, B-9000 Ghent, Belgium
e-mail: {Joris.Degroote,Sebastiaan.Annerel,Jan.Vierendeels}@UGent.be

Key words: Fluid-structure interaction, stability, tube, time step, Gauss-Seidel, quasi-Newton

Abstract. *In partitioned simulations of fluid-structure interaction (FSI), the flow equations and the structural equations are solved with separate solvers. If the interaction between the flow and the flexible structure is strong, coupling iterations between both solvers have to be performed in each time step. In previous work, a Fourier stability analysis of Gauss-Seidel coupling iterations was presented for the unsteady, incompressible flow in a straight flexible tube. The error on the displacement of the fluid-structure interface during the coupling iterations was decomposed as a sum of Fourier modes. Subsequently, the amplification of each Fourier error mode was determined analytically as a function of a dimensionless time step τ and a dimensionless stiffness κ. However, the structural model in this analysis was an independent-rings model without inertia.*

Recently, this Fourier stability analysis has been extended with a more complex structural model. The structural inertia and the interaction between the tube segments are now taken into account. It has been observed that the interaction between the tube segments reduces the amplification factor of the Fourier error modes compared to the independent-rings model. Moreover, the number of unstable modes is only influenced by τ for a range of τ if the structural inertia is substantial while it increases indefinitely as τ decreases if the structural inertia is negligible. These tendencies are confirmed by numerical experiments with the quasi-Newton IQN-ILS algorithm. As expected, numerical experiments with Gauss-Seidel iterations for the entire range of τ are impossible due to the presence of unstable modes. In conclusion, the stability analysis of coupling iterations in partitioned FSI simulations is strongly influenced by the structural model.

1 INTRODUCTION

The interaction of a fluid with a flexible structure can be simulated in either a monolithic or a partitioned way. The monolithic approach is to solve the governing equations of the flow and the structural displacement simultaneously whereas in a partitioned simulation the flow and the structural deformation are calculated separately. Generally, a Dirichlet-Neumann decomposition of the coupled problem is employed which means that a velocity (or displacement) is imposed as boundary condition on the fluid-structure interface when solving the flow equations and that a stress is imposed on the interface when solving the structural equations.

For a partitioned simulation of strong interaction between the fluid and the structure, e.g. blood flow in a flexible artery, a coupling algorithm is required to find the displacement of the interface for which the stresses on both sides of the interface are in equilibrium. The most rudimentary coupling algorithm for a black-box flow solver and structural solver uses Gauss-Seidel iterations, which means that the flow equations and the structural equations are solved successively until convergence is reached. However, Gauss-Seidel iterations often converge slowly, if at all. The convergence of the Gauss-Seidel coupling iterations depends on several parameters, such as the geometry, the time step, the structural stiffness and the ratio of the fluid density to the structural density. For other partitioned techniques, the exact relation between these parameters and the convergence of the coupling iterations will be different but the tendencies are expected to be similar. Consequently, it is useful to analyze the convergence behaviour of coupling with Gauss-Seidel iterations as a function of these parameters.

A stability analysis is the obvious means to gain a clear understanding of a partitioned technique's behaviour. Previously, such a stability analysis has been performed by Förster et al. [5] who analyzed the effect of the aforementioned parameters on algorithms without coupling iterations. Causin et al. [2] studied algorithms with and without coupling iterations using Dirichlet-Neumann and Neumann-Dirichlet decomposition. They derived the maximal relaxation factor that leads to convergence of the coupling iterations as a function of these parameters for a simplified model of blood flow in an artery and then validated the formulas with numerical experiments. Later, Badia et al. [1] derived the relaxation factor for the same case but with Robin-Dirichlet and Robin-Neumann decomposition. Vierendeels et al. [11] analyzed the stability of coupling iterations for the one-dimensional motion of a rigid object in a channel as a function of the density ratio and the size of the gap between the object and the channel. In their model, the structure only has inertia and no stiffness. Consequently, the inertia of the fluid and of the structure are balancing each other out, which results in an error amplification factor of the coupling iterations that is independent of the time step. The difference between compressible and incompressible fluids is analyzed by van Brummelen [10] for the partitioned simulation of the flow over a flexible panel.

In this article, a Fourier stability analysis is performed on Gauss-Seidel coupling iterations, also for a simplified model of blood flow in an artery. This analysis results in a modal decomposition of the error on the interface's displacement during Gauss-Seidel coupling iterations and the error amplification factor that corresponds with each Fourier mode. Such a modal de-

composition provides more information than a single relaxation factor and explains the fast convergence of the interface block quasi-Newton method with approximate Jacobians from least-squares models (IBQN-LS[12]) and the interface quasi-Newton method with approximation for the inverse of the Jacobian from a least-squares model (IQN-ILS[3]).

The blood flow in an artery is modelled as the unsteady, incompressible flow in a straight, elastic tube. The structural model includes both the interaction between the segments of the tube and the structural inertia as opposed to previous work[4] in which this stability analysis was performed with a simple structural model that consisted of independent segments without structural inertia. The improved structural model leads to important new insights, among others with regard to the effect of the time step.

The model is one-dimensional to enable both analytical and numerical analysis. A one-dimensional model behaves similarly to two-dimensional (axisymmetric) and three-dimensional models from a fluid-structure interaction point of view although it does by no means reflect all complex phenomena in a real artery. Moreover, a one-dimensional model is perfectly suited for analyzing the effect of the aforementioned parameters on the number of coupling iterations. However, the Fourier stability analysis considers the linearized equations without boundary conditions. Therefore, its conclusions need to be verified with simulations of the original non-linear equations over a wide range of the parameters. Because Gauss-Seidel coupling iterations are often unstable for the parameter values of interest, another coupling algorithm, in this case IQN-ILS, is used for these verification simulations.

The remainder of this article is organized as follows. Section 2 describes the governing equations for the fluid and the structure as well as their discretization. The Fourier stability analysis follows in Section 3 and the results of the stability analysis are verified in Section 4 by means of numerical experiments.

2 DESCRIPTION OF THE MODEL

2.1 Governing equations

The flow in an artery is simplified to the unsteady, incompressible flow in a straight, flexible tube with a circular cross-section and length L, depicted in Figure 1. The model is one-dimensional and gravity and viscosity are not taken into account. The flow is governed by the continuity and momentum equation which can be written in conservative form as

$$\frac{\partial a}{\partial t} + \frac{\partial av}{\partial z} = 0 \tag{1a}$$

$$\frac{\partial av}{\partial t} + \frac{\partial av^2}{\partial z} + \frac{1}{\rho_f}\left(\frac{\partial ap'}{\partial z} - p'\frac{\partial a}{\partial z}\right) = 0 \tag{1b}$$

with z the coordinate along the axis of the tube, $a = \pi r^2$ the cross-sectional area of the tube and r the inner radius. t is the time, v the velocity along the axis of the tube, p' the pressure and ρ_f the density of the fluid. The kinematic pressure $p = p'/\rho_f$ is referred to as the pressure in the remainder of this article. At the inlet of the tube, the velocity is imposed and a pressure boundary is prescribed at the outlet.

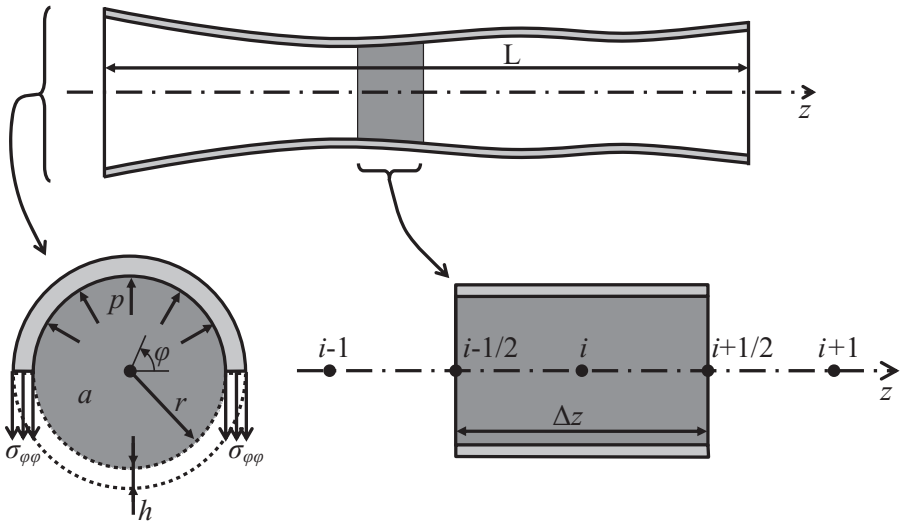

Figure 1: The model for blood flow in an artery with details of the cross-section and a control volume used in the discretization of the governing equations.

The structural model in the previous work[4] disregards the mass of the structure. Moreover, it is a so-called independent-rings model[9] because the interaction between the segments of the tube is not taken into account. In this paper, the model of the tube's wall is improved by including the structural mass and the interaction between the segments. An axisymmetric model is used in the coordinate system (r,φ,z), with φ the angle in the cross-sectional plane as indicated in Figure 1. The structural deformation in the radial direction is determined by

$$\rho_s h \frac{\partial^2 r}{\partial t^2} + A \frac{\partial^4 r}{\partial z^4} - B \frac{\partial^2 r}{\partial z^2} + C\,(r - r_o) = \rho_f\,(p - p_o) \tag{2}$$

with ρ_s the solid density and h the thickness of the tube's wall[9]. Axial deformations of the structure are not considered so the length of a tube segment remains constant. The parameters A and B ($A, B \geq 0$) account for the inner action of the bending and the tension in the tissue, and they depend on the properties of the structure. The parameter C is equal to $\frac{Eh}{r_o^2(1-\nu^2)}$ with E the Young's modulus and ν the Poisson coefficient. This expression for C corresponds with a tube that is clamped in the axial direction. The radius r_o corresponds to a uniform pressure p_o if the structure is at rest.

2.2 Discretization

The straight tube with circular cross-section and length L is discretized using a one-dimensional grid with N cells of length Δz, as indicated in Figure 1. The fluid velocity and pressure are

stored in the cell centres. Central discretization is used for all terms in the continuity and momentum equation, except for the convective term in the momentum equation which is discretized with a first-order upwind scheme. The time discretization scheme is backward Euler and the time step is indicated with Δt. The conservation of mass and momentum in a control volume around cell centre i is expressed by the following system of equations

$$\frac{\Delta z}{\Delta t}\left(a_i - a_i^n\right) + v_{i+1/2}a_{i+1/2} - v_{i-1/2}a_{i-1/2} - \alpha\left(p_{i+1} - 2p_i + p_{i-1}\right) = 0 \tag{3a}$$

$$\frac{\Delta z}{\Delta t}\left(v_i a_i - v_i^n a_i^n\right) + v_i v_{i+1/2}a_{i+1/2} - v_{i-1}v_{i-1/2}a_{i-1/2} + \frac{1}{2}\left[a_{i+1/2}\left(p_{i+1} - p_i\right) + a_{i-1/2}\left(p_i - p_{i-1}\right)\right] = 0 \tag{3b}$$

for $v_i \geq 0$. The subscripts i, $i+1$ and $i-1$ indicate the cell centres ($i = 1, \ldots, N$) and the subscript $i \pm 1/2$ signifies the values calculated at the cell interfaces, $v_{i-1/2} = (v_{i-1} + v_i)/2$ and $v_{i+1/2} = (v_i + v_{i+1})/2$. The superscript n denotes the previous time level; the superscript $n+1$ for the new time level is omitted. A pressure stabilization term with coefficient $\alpha = a_o/\left(v_o + \Delta z/\Delta t\right)$ has been added in the continuity equation to prohibit pressure wiggles due to central discretization of the pressure in the momentum equation, with v_o the reference flow velocity. This stabilization term can be written as

$$\frac{a_o}{v_o + \Delta z/\Delta t}\left(\Delta z^2 \left.\frac{\partial^2 p}{\partial z^2}\right|_i + O\left(\Delta z^4\right)\right) \tag{4}$$

on Cartesian grids. In Eq. (3a), the first term and the combination of the second and the third term are proportional to Δz but they do not scale with Δt. For large Δt, the stabilization term is proportional to Δz^2 so it scales with Δz with respect to the other terms in Eq. (3a); for small Δt, the stabilization term is proportional to $\Delta t \Delta z$ so it scales with Δt with respect to the other terms. Thus, the stabilization term does not affect the accuracy of the scheme because the other terms are also first-order accurate. This stabilization term can also be implementated with higher-order accuracy on non-Cartesian grids using a finite volume discretization[13].

As mentioned above, the velocity at the inlet and the pressure at the outlet are imposed as a function of time. The pressure at the inlet and the velocity at the outlet are linearly extrapolated

$$p_{in} = 2p_1 - p_2 \tag{5a}$$

$$v_{out} = 2v_N - v_{N-1}. \tag{5b}$$

The geometrical discretization of the structural problem is identical to that of the flow problem to avoid interpolation errors. The structural equation (Eq. (2)) is discretized in space with

the central difference method and in time with the Newmark method[8], giving

$$\frac{\rho_s h}{\beta \Delta t^2} r_i + \frac{A}{\Delta z^4}\left(r_{i+2} - 4r_{i+1} + 6r_i - 4r_{i-1} + r_{i-2}\right) - \frac{B}{\Delta z^2}\left(r_{i+1} - 2r_i + r_{i-1}\right) + C\left(r_i - r_o\right)$$
$$= \rho_f\left(p_i - p_o\right) + \rho_s h\left[\frac{1}{\beta \Delta t^2} r_i^n + \frac{1}{\beta \Delta t}\dot{r}_i^n + \left(\frac{1}{2\beta} - 1\right)\ddot{r}_i^n\right] \quad (6a)$$

for cell i ($i = 1, \ldots, N$). An overdot signifies a time derivative and the superscript n refers to values from the previous time step. Once the solution at time step $n+1$ has been found, the corresponding acceleration and velocity are calculated as

$$\ddot{r}_i^{n+1} = \frac{1}{\beta \Delta t^2}\left(r_i^{n+1} - r_i^n\right) - \frac{1}{\beta \Delta t}\dot{r}_i^n - \left(\frac{1}{2\beta} - 1\right)\ddot{r}_i^n \quad (6b)$$

$$\dot{r}_i^{n+1} = \dot{r}_i^n + \Delta t\left(1 - \gamma\right)\ddot{r}_i^n + \Delta t \gamma \ddot{r}_i^{n+1}. \quad (6c)$$

The Newmark parameters β and γ are chosen so that $\gamma \geq \frac{1}{2}$ and $\beta \geq \frac{1}{4}\left(\frac{1}{2} + \gamma\right)^2$, which results in an unconditionally stable integration scheme.

2.3 Gauss-Seidel coupling iterations

A scheme with Gauss-Seidel iterations to calculate the fully coupled solution for time step $n+1$ is described below, with a superscript k or $k+1$ to indicate the coupling iteration within time step $n+1$.

1. Solve Eqs. (3) for the new velocity v_i^{k+1} and pressure p_i^{k+1} with a given geometry r_i^k ($i = 1, \ldots, N$).
2. Solve Eq. (6a) for the new geometry r_i^{k+1} with the pressure p_i^{k+1} from the preceding step ($i = 1, \ldots, N$).
3. (a) If converged, go to the next time level.
   (b) Otherwise, increase k and go to step 1.

This coupling scheme does not perform well in most cases with strong interaction between fluid and structure. If this iteration scheme converges, often a large number of coupling iterations is needed. In the numerical experiments, the position of the fluid-structure interface at the beginning of the first coupling iteration is calculated with an extrapolation from the previous time steps

$$r_i^{n+1,0} = \frac{5}{2} r_i^n - 2 r_i^{n-1} + \frac{1}{2} r_i^{n-2}, \quad (7)$$

which is third-order accurate if the time step Δt is constant. However, this extrapolation does not influence the stability analysis in the following section.

3 FOURIER STABILITY ANALYSIS

3.1 Linearization

The stability of the Gauss-Seidel coupling algorithm is now determined with Fourier stability analysis on the flow equations and the structural equations. The velocity, pressure and inner radius of the tube in Eqs. (3) and Eqs. (6) are substituted by the sum of the coupled solution and the remaining error in the coupling iteration (indicated with a tilde). The coupled solution at both time level n and $n+1$ is in turn linearized as the sum of the reference value (subscript o) and a perturbation (indicated with a hat). For the velocity, this gives

$$v_i^k = v_o + \hat{v}_i + \tilde{v}_i^k \tag{8}$$

for $i = 1, \ldots, N$ and analogously for the pressure and the inner radius. Subsequently, a is replaced by πr^2 and all equations are linearized by neglecting the nonlinear combinations of the error terms and the perturbations. Because the equations linearized around v_o, p_o and r_o are satisfied by the coupled solution, all perturbations from the current and previous time step cancel out, which results in the following equations for the error terms

$$\frac{\Delta z}{\Delta t} 2 r_o \tilde{r}_i^k + 2 v_o r_o \left(\tilde{r}_{i+1/2}^k - \tilde{r}_{i-1/2}^k\right) + r_o^2 \left(\tilde{v}_{i+1/2}^{k+1} - \tilde{v}_{i-1/2}^{k+1}\right) - \alpha' \left(\tilde{p}_{i+1}^{k+1} - 2\tilde{p}_i^{k+1} + \tilde{p}_{i-1}^{k+1}\right) = 0 \tag{9a}$$

$$\frac{\Delta z}{\Delta t} \left(2 v_o r_o \tilde{r}_i^k + r_o^2 \tilde{v}_i^{k+1}\right) + 2 v_o^2 r_o \left(\tilde{r}_{i+1/2}^k - \tilde{r}_{i-1/2}^k\right) + v_o r_o^2 \left(\tilde{v}_{i+1/2}^{k+1} + \tilde{v}_i^{k+1} - \tilde{v}_{i-1/2}^{k+1} - \tilde{v}_{i-1}^{k+1}\right) + \frac{r_o^2}{2} \left(\tilde{p}_{i+1}^{k+1} - \tilde{p}_{i-1}^{k+1}\right) = 0 \tag{9b}$$

$$\frac{\rho_s h}{\beta \Delta t^2} \tilde{r}_i^{k+1} + \frac{A}{\Delta z^4} \left(\tilde{r}_{i+2}^{k+1} - 4\tilde{r}_{i+1}^{k+1} + 6\tilde{r}_i^{k+1} - 4\tilde{r}_{i-1}^{k+1} + \tilde{r}_{i-2}^{k+1}\right) - \frac{B}{\Delta z^2} \left(\tilde{r}_{i+1}^{k+1} - 2\tilde{r}_i^{k+1} + \tilde{r}_{i-1}^{k+1}\right) + C \tilde{r}_i^{k+1} = \rho_f \tilde{p}_i^{k+1} \tag{9c}$$

with $\alpha' = \alpha/\pi$. Because Eq. (6b) and Eq. (6c) are only used at the end of the time step, they are not important for the stability of the coupling iterations within the time step. This means that γ is not a parameter in these iterations.

The error terms are expanded as the sum of N Fourier modes, giving

$$\tilde{v}_i^k = \frac{1}{N} \sum_{\ell=0}^{N-1} \check{v}_\ell^k \exp\left(\jmath \omega_\ell i \Delta z\right) \tag{10}$$

for the error on the velocity ($i = 1, \ldots, N$) with $\jmath = \sqrt{-1}$ and $\omega_\ell = \frac{2\pi\ell}{L}$ the (angular) wave number. As the error terms $\tilde{v}_i^k$ are real, half of the complex coefficients $\check{v}_\ell^k$ are redundant as they satisfy

$$\check{v}_\ell^k = \left(\check{v}_{N-\ell}^k\right)^* \tag{11}$$

with a star to denote complex conjugation. Therefore, only half of the complex coefficients $\check{v}_\ell^k$ actually need to be calculated. If N is even, these coefficients are calculated for $\ell = 0, 1, \ldots, N/2$; if N is odd, they are calculated for $\ell = 0, 1, \ldots, (N-1)/2$.

The amplification of each wave number can be studied separately as Eqs. (9) are linear in $\tilde{v}$, $\tilde{p}$ and $\tilde{r}$. Therefore, $\tilde{v}_i^k$ is substituted by $\check{v}_\ell^k \exp(\jmath\omega_\ell i\Delta z)$ and analogously for the error on the pressure and the radius. The product $\omega_\ell\Delta z$ is denoted as the dimensionless wave number ϑ_ℓ. For clarity, the inverted hat and the subscript ℓ are omitted.

$$\frac{\Delta z}{\Delta t} 2r_o r^k + 2v_o r_o \jmath \sin(\vartheta) r^k + r_o^2 \jmath \sin(\vartheta) v^{k+1} + 2\alpha' \left(1 - \cos(\vartheta)\right) p^{k+1} = 0 \tag{12a}$$

$$\begin{aligned}\frac{\Delta z}{\Delta t}\left(2v_o r_o r^k + r_o^2 v^{k+1}\right) + 2v_o^2 r_o \jmath \sin(\vartheta) r^k \\ + v_o r_o^2 \left(1 + \jmath\sin(\vartheta) - \exp(-\jmath\vartheta)\right) v^{k+1} + r_o^2 \jmath \sin(\vartheta) p^{k+1} = 0\end{aligned} \tag{12b}$$

$$\left[\frac{\rho_s h}{\beta\Delta t^2} + \frac{4A}{\Delta z^4}\left(1 - \cos(\vartheta)\right)^2 + \frac{2B}{\Delta z^2}\left(1 - \cos(\vartheta)\right) + C\right] r^{k+1} = \rho_f p^{k+1} \tag{12c}$$

3.2 Amplification factor

By combining Eqs. (12), the amplification factor μ of each mode in the error on the radius or on the pressure is calculated as

$$\mu = \left|\frac{r^{k+1}}{r^k}\right| = \left|\frac{p^{k+1}}{p^k}\right| = |\mu_1 \mu_2| \tag{13a}$$

with

$$\mu_1 = \frac{\frac{\rho_f}{\rho_s}}{\begin{array}{c}\frac{\rho_f r_o^2\left(1-\nu^2\right)}{E\beta\Delta t^2} + \frac{4Ar_o^2\left(1-\nu^2\right)}{Eh\Delta z^4}\frac{\rho_f}{\rho_s}\left(1 - \cos(\vartheta)\right)^2 \\ + \frac{2Br_o^2\left(1-\nu^2\right)}{Eh\Delta z^2}\frac{\rho_f}{\rho_s}\left(1 - \cos(\vartheta)\right) + \frac{\rho_f}{\rho_s}\end{array}} \tag{13b}$$

and

$$\mu_2 = \frac{\rho_f r_o \left(1 - \nu^2\right)}{Eh} \cdot \frac{\begin{array}{c}\left(2\frac{\Delta z}{\Delta t} v_o \jmath \sin(\vartheta) - 2v_o^2 \sin^2(\vartheta)\right) \\ - \left[\frac{\Delta z}{\Delta t} + v_o\left(\jmath\sin(\vartheta) + 1 - \exp(-\jmath\vartheta)\right)\right] \\ \cdot \left(2\frac{\Delta z}{\Delta t} + 2v_o \jmath \sin(\vartheta)\right)\end{array}}{\begin{array}{c}\left[\frac{\Delta z}{\Delta t} + v_o\left(\jmath\sin(\vartheta) + 1 - \exp(-\jmath\vartheta)\right)\right] \\ \cdot \left[\frac{2}{v_o + \Delta z/\Delta t}\left(1 - \cos(\vartheta)\right)\right] + \sin^2(\vartheta)\end{array}}. \tag{13c}$$

The coefficient α' of the pressure stabilization term in the continuity equation has been substituted by

$$\alpha' = \frac{r_o^2}{v_o + \Delta z/\Delta t} \tag{14}$$

in the previous equation because α' cannot be altered independently.

The dimensionless stiffness κ and dimensionless time step τ have the same meaning as in previous work[3]. An additional dimensionless parameter ϕ accounts for the structural inertia, giving

$$\kappa = \frac{c_o}{v_o} \qquad \tau = \frac{v_o \Delta t}{L} \qquad N = \frac{L}{\Delta z} \qquad \phi = \frac{r_o v_o}{\Delta z w_o} \tag{15a}$$

with

$$c_o = \sqrt{\frac{Eh}{2 r_o \rho_f \left(1-\nu^2\right)}} \qquad w_o = \sqrt{\frac{E\beta}{\rho_s \left(1-\nu^2\right)}}. \tag{15b}$$

The interaction between the segments is determined by the parameters

$$\chi = \frac{4 A r_o^2 \left(1-\nu^2\right)}{Eh\Delta z^4} \qquad \psi = \frac{2 B r_o^2 \left(1-\nu^2\right)}{Eh\Delta z^2}. \tag{15c}$$

With these definitions, the error amplification factor is given by $\mu = |\mu_1 \mu_2|$ with

$$\mu_1 = \frac{1}{\left(\frac{\phi}{\tau N}\right)^2 + \chi \left(1-\cos(\vartheta)\right)^2 + \psi \left(1-\cos(\vartheta)\right) + 1} \tag{16a}$$

and

$$\mu_2 = \frac{1}{\kappa^2} \frac{\begin{array}{c}(\tau N)^3 \left(1-\exp\left(-\jmath\vartheta\right)\right) \jmath \sin(\vartheta) \\ +(\tau N)^2 \left[\jmath \sin(\vartheta) + \left(1-\exp\left(-\jmath\vartheta\right)\right)\left(1+\jmath\sin(\vartheta)\right)\right] \\ +\tau N \left(\jmath\sin(\vartheta) + 2 - \exp\left(-\jmath\vartheta\right)\right) + 1\end{array}}{\begin{array}{c}(\tau N)^3 \left[\sin^2(\vartheta) + 2\left(\jmath\sin(\vartheta) + 1 - \exp\left(-\jmath\vartheta\right)\right)\left(1-\cos(\vartheta)\right)\right] \\ +(\tau N)^2 \left[\sin^2(\vartheta) + 2\left(1-\cos(\vartheta)\right)\right]\end{array}}. \tag{16b}$$

The expression for μ_2 above is identical to the error amplification factor in previous work[4] which was derived using a simple structural model with independent tube segments and no structural inertia. The structural model that is presented in this article (Eq. (2)) with interaction between the segments and with structural inertia results in additional contributions to the error amplification which are all grouped in a new term μ_1. Consequently, the complete error amplification factor is obtained as the product of μ_1 and μ_2. The results of the previous analysis are thus confirmed and the conclusions remain valid.

3.3 Discussion

Because $(1-\cos(\vartheta))$ is never negative and $\left(\frac{\phi}{\tau N}\right)^2+1$ is always positive, the second and third term in the denominator of μ_1 never increase the error amplification ($\chi,\psi\geq 0$). The error amplification will thus always be mitigated by increasing the parameters χ and ψ which account for the interaction between the tube segments. Taking into account the interaction between the tube segments in the structural model should therefore facilitate the convergence of the coupling iterations compared to a simulation with an independent-rings model. Because both χ and ψ appear only once in the expression for μ, it is easy to understand their effect and consequently they can be set to zero in the remainder of the analysis. With $\chi=\psi=0$, μ_1 is independent of the wave number.

The effect of the time step on the stability is important in many cases and it is more complex. The factor μ_1 is proportional to $(\tau N)^2$ if $\tau N \ll \phi$ and if the relative contribution of the terms due to the interaction between the tube segments is small. If $\tau N \ll 1$ then μ_2 is proportional to $(\tau N)^{-2}$; otherwise τN only influences μ_2 for the lowest and highest wave numbers ($\vartheta \approx 0$ or π). Apart from $\tau N \approx 1$ and $\tau N \approx \phi$ which are difficult to analyze, there are three possibilities for the effect of the time step on the stability of the coupling iterations in this particular case:

- $\mu \sim (\tau N)^2$: if $\tau N \ll \phi$ and $\tau N \gg 1$;
- $\mu \approx \text{constant}$: if both $\tau N \ll \phi$ and $\tau N \ll 1$ or if both $\tau N \gg \phi$ and $\tau N \gg 1$;
- $\mu \sim (\tau N)^{-2}$: if $\tau N \gg \phi$ and $\tau N \ll 1$.

If the time step is varied over a wide range, its effect on μ might change throughout that variation as the time step determines which of the above situations is appropriate. The time step will have no significant influence on the error amplification factor μ if τN is sufficiently far outside the range

$$\left[\min\left(1,\phi\right),\max\left(1,\phi\right)\right]. \tag{17}$$

If $\phi<1$ then μ is proportional to $(\tau N)^{-2}$ when τN lies in the range given above. By contrast, if $\phi>1$ then μ is proportional to $(\tau N)^2$ for τN in that range.

If $\tau N \ll 1$, the inertia is dominant in the flow while if $\tau N \gg 1$, the flow almost reaches steady state in each time step. For the structure, the inertia is dominant if $\tau N \ll \phi$ while the stiffness is dominant if $\tau N \gg \phi$. Hence, the inertia in the fluid and in the structure are balancing each other out if $\tau N \ll 1$ and $\tau N \ll \phi$. For $\tau N \ll 1$ and $\tau N \gg \phi$, an equilibrium between the inertia in the fluid and the structural stiffness has to be found. By contrast, $\tau N \gg 1$ and $\tau N \ll \phi$ results in an equilibrium between the structural inertia and the fluid which can be considered to be at steady state. Finally, if $\tau N \gg 1$ and $\tau N \gg \phi$, then inertia is insignificant in both the fluid and the structure. So, if inertia is important in either the fluid or the structure, then the error amplification factor μ is proportional to $(\tau N)^{-2}$ or $(\tau N)^2$, respectively.

Figure 2 depicts the evolution of μ as function of τN with parameters that approximate the flow in a piece of a large artery (see Table 1) such that $\phi \approx 0.1$ and $\kappa \approx 60$. It can be seen that μ is proportional to $(\tau N)^{-2}$ for $\tau N \in [0.1, 1]$ and constant for τN outside that range.

Figure 3 shows μ as a function of the wave number for four different values of τN. Once more, an increase in μ can be noticed for decreasing τN as long as $\tau N \in [0.1, 1]$ and much smaller changes for τN outside that range. In all figures, the stability limit ($\mu = 1$) is marked with a horizontal dotted line and the range $[0.1, 1]$ is bounded by vertical dotted lines when applicable.

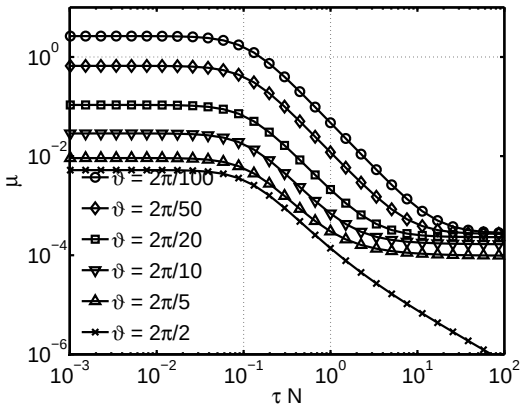

Figure 2: The error amplification factor as a function of τN for different values of the wave number ϑ.

L	=	0.050 m	E	=	300000 N/m^2	β	=	1/4
h	=	0.001 m	ν	=	0.4	γ	=	1/2
r_o	=	0.005 m	ρ_f	=	1000 kg/m^3	δ	=	1/2
v_o	=	0.1 m/s	ρ_s	=	1200 kg/m^3	N	=	100

Table 1: The parameter values that are used to model blood flow in a piece of a large artery.

The error amplification factor for the low wave numbers still depends somewhat on the time step's size when $\tau N \notin [0.1, 1]$ in Figure 2, especially for $\tau N > 1$. For the highest wave number ($\vartheta = \pi$), the influence of the time step's size remains present when τN goes to infinity. As mentioned above, μ_2 is still influenced by τN for the lowest and highest wave numbers ($\vartheta \approx 0$ or π) when $\tau N \gg 1$.

When $\tau N \ll \phi$, μ_1 is proportional to ϕ^{-2} and μ_2 always holds a factor κ^{-2} such that μ is proportional to $(\phi\kappa)^{-2}$, which contains the ratio of the fluid density to the solid density ρ_f/ρ_s. As expected, increasing this ratio increases the error amplification factor.

The number of unstable modes as a function of the dimensionless time step is depicted in Figure 4 for $N = 100$. While the error amplification factor μ as a function of ϑ depends on τN, the number of modes with $\mu > 1$ is mainly a function of τ alone but the boundaries of the region $\tau N = [0.1, 1]$ in which the number of unstable modes increases for decreasing τ depend on N.

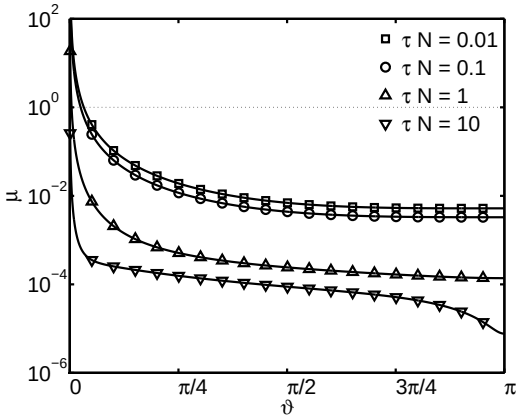

Figure 3: The error amplification factor as a function of the wave number ϑ for different values of τN.

4 NUMERICAL EXPERIMENTS

Nonlinear simulations of the flow in a flexible tube are used to verify the conclusions of the linear analysis, especially with regard to the effect of the time step as this effect is the most important one. A velocity of

$$v_{in} = v_o + \frac{v_o}{100} \sin\left(2\pi n \tau\right) \tag{18}$$

has been applied at the inlet of the tube and zero pressure is imposed at the outlet of the tube ($p_{out} = 0$). The structure is initially at rest and both χ and ψ have been set to zero. The tube is discretized in $N = 100$ segments with the same length. The values from Table 1 have been used again for the geometry and for the properties of the materials. For these values, the stability analysis predicts that the error amplification factor μ will increase for a decreasing τN in the range $[0.1, 1]$, that μ will be more or less constant outside this range (see Figure 2) and that the number of unstable modes has a similar behaviour (see Figure 4).

Simulations with 100 time steps have been performed for different values of τ and with different coupling algorithms. The L^2-norm of the residual is reduced by three orders of magnitude with respect to its initial value in the time step. In Figure 5, the average number of coupling iterations per time step is depicted for different sizes of the dimensionless time step τ and the range $[0.1/N, 1/N]$ is indicated with vertical dotted lines.

Figure 3 shows that the error amplification is smaller than one for all wave numbers if the time step is large ($\tau \approx 1$), except for $\vartheta = 0$. As a result, Figure 4 indicates one unstable mode for $\tau \approx 1$. Although Gauss-Seidel iterations are expected to diverge if $\mu > 1$ for at least one mode, they converge quickly for a large time step ($\tau \approx 1$). This discrepancy is caused by the boundary conditions which are not taken into account in the stability analysis. By imposing the pressure at the outlet and with a wall model $a = a(p)$, the components of the error on p and a with $\vartheta = 0$ are also determined, so this unstable mode is stabilized by the boundary conditions.

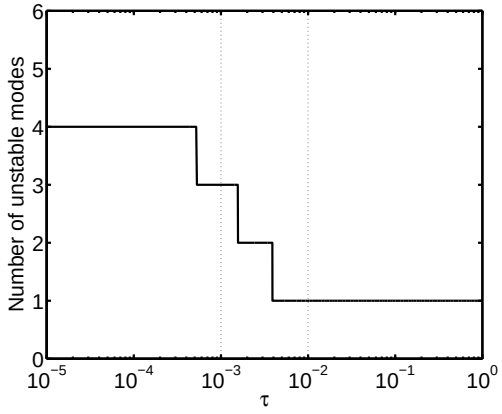

Figure 4: The number of unstable Fourier modes as a function of the dimensionless time step τ with $N = 100$.

When the time step decreases, the convergence of the Gauss-Seidel iterations becomes slow; for example, on average 28 Gauss-Seidel coupling iterations per time step were required for a dimensionless time step of $\tau = 2 \times 10^{-2}$. The Gauss-Seidel iterations diverged in the first time step when τ was less than or equal to 10^{-2}.

It is thus impossible to verify the conclusions of the stability analysis over a wide range of time steps by performing simulations with the Gauss-Seidel coupling algorithm because the error amplification factor for the low wave numbers would be larger than one in the simulations with a small time step, which would cause divergence of the Gauss-Seidel coupling iterations. Other coupling algorithms, such as IQN-ILS[3] or Gauss-Seidel iterations with (dynamic) relaxation[6,7], have to be used for the partitioned simulations with small time steps. The IQN-ILS algorithm uses information from the previous coupling iterations in the current time step to approximate the inverse of the Jacobian of the coupled problem written as a root-finding equation. The IQN-ILS algorithm behaves like a Newton algorithm for the part of the residual that can be decomposed as a linear combination of differences between the values in previous coupling iterations and like Gauss-Seidel iterations for the other part. The number of IQN-ILS coupling iterations per time step (averaged over the 100 time steps in the simulation) is a measure for the number of unstable modes[3].

Figure 5 shows that the number of IQN-ILS coupling iterations per time step is almost constant for $\tau = 6 \times 10^{-1}$ to 6×10^{-2} and for $\tau = 2 \times 10^{-4}$ to 2×10^{-5}. Between $\tau = 6 \times 10^{-2}$ and 2×10^{-4}, the number of IQN-ILS iterations increases steadily with decreasing time step. Consequently, the number of IQN-ILS coupling iterations per time step (Figure 5) and the number of unstable modes (Figure 4) display a similar behaviour.

The increase in the number of IQN-ILS coupling iterations with a decreasing time step can be mitigated by using information from the coupling iterations in the previous time steps as well, instead of only information from the current time step. Figure 5 illustrates that the number

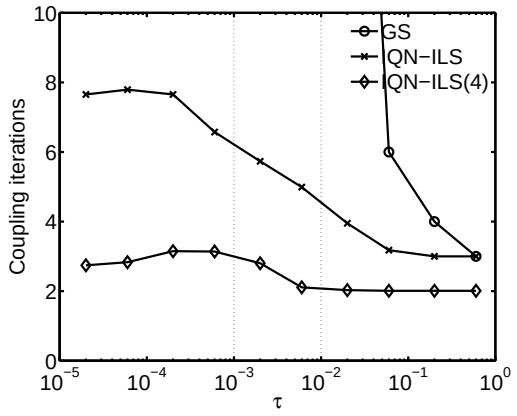

Figure 5: The number of coupling iterations per time step (averaged over 100 time steps) for different values of τ with $N = 100$. As predicted by the stability analysis, the average number of IQN-ILS coupling iterations per time step increases as τ decreases for τ in the range $[10^{-3}, 10^{-2}]$ while it is constant for τ sufficiently far outside that range. Reuse of information from the 4 previous time steps (IQN-ILS(4)) mitigates the increase of the average number of coupling iterations as τ decreases.

of coupling iterations per time step is reduced significantly if the information from the four previous time steps, denoted as IQN-ILS(4), is also used.

5 CONCLUSIONS

Fourier stability analysis has been performed on Gauss-Seidel iterations between the flow solver and the structural solver for the flow in a flexible tube with interacting segments and structural inertia. The error amplification factor is reduced compared to the independent-rings model by including the interaction between the segments of the tube in the structural model. For parameter values that approximate the flow in a piece of a large artery, the error amplification factor of Gauss-Seidel coupling iterations increases if the time step's size decreases, but only within a certain range of the time step's size. Outside this range, the time step has little effect on the error amplification factor. The stability analysis of the Gauss-Seidel iterations is confirmed by the variation in the number of IQN-ILS coupling iterations as a function of the time step's size in nonlinear simulations.

ACKNOWLEDGMENTS

J. Degroote gratefully acknowledges a Ph.D. fellowship of the Research Foundation - Flanders (FWO).

REFERENCES

[1] S. Badia, F. Nobile and C. Vergara, Fluid-structure partitioned procedures based on Robin transmission conditions, *Journal of Computational Physics*, **227**, 7027–7051 (2008).

[2] P. Causin, J.-F. Gerbeau and F. Nobile, Added-mass effect in the design of partitioned algorithms for fluid-structure problems, *Computer Methods in Applied Mechanics and Engineering*, **194**, 4506–4527 (2005).

[3] J. Degroote, K.-J. Bathe and J. Vierendeels, Performance of a new partitioned procedure versus a monolithic procedure in fluid-structure interaction, *Computers & Structures*, **87**, 793–801 (2009).

[4] J. Degroote, P. Bruggeman, R. Haelterman and J. Vierendeels, Stability of a coupling technique for partitioned solvers in FSI applications, *Computers & Structures*, **86**, 2224–2234 (2008).

[5] C. Förster, W. Wall and E. Ramm, Artificial added mass instabilities in sequential staggered coupling of nonlinear structures and incompressible viscous flows, *Computer Methods in Applied Mechanics and Engineering*, **196**, 1278–1293 (2007).

[6] U. Küttler and W. Wall, Fixed-point fluid-structure interaction solvers with dynamic relaxation, *Computational Mechanics*, **43**, 61–72 (2008).

[7] D. Mok and W. Wall, Partitioned analysis schemes for the transient interaction of incompressible flows and nonlinear flexible structures, in K. Schweizerhof, W. Wall and K.-U. Bletzinger (Eds.), Trends in computational structural mechanics, Barcelona (2001).

[8] N. Newmark, A method of computation for structural dynamics, *ASCE Journal of the Engineering Mechanics Division*, **85**, 67–94 (1959).

[9] A. Quarteroni, M. Tuveri and A. Veneziani, Computational vascular fluid dynamics: problems, models and methods, *Computing and Visualization in Science*, **2**, 163–197 (2000).

[10] E. van Brummelen, Added mass effects of compressible and incompressible flows in fluid-structure interaction, *Journal of Applied Mechanics*, **76**, 021206–1–7 (2009).

[11] J. Vierendeels, K. Dumont, E. Dick and P. Verdonck, Analysis and stabilization of fluid-structure interaction algorithm for rigid-body motion, *AIAA Journal*, **43**, 2549–2557 (2005).

[12] J. Vierendeels, L. Lanoye, J. Degroote and P. Verdonck, Implicit coupling of partitioned fluid-structure interaction problems with reduced order models, *Computers & Structures*, **85**, 970–976 (2007).

[13] J. Vierendeels, K. Riemslagh and E. Dick, A multigrid semi-implicit line-method for viscous incompressible and low-Mach-number flows on high aspect ratio grids, *Journal of Computational Physics*, **154**, 310–341 (1999).